



## Optimized Prediction of Airflow Volume in Under-Actuated Zones through Multilayer Perceptron Artificial Neural Network

Yaddarabullah<sup>1\*</sup>    Abiyyu Muhammad Arif<sup>1</sup>    Dewi Lestari<sup>1</sup>    Budi Arifitama<sup>1</sup>  
 Dina Nurul Fitria<sup>2</sup>    Erneza Dewi Krishnasari<sup>3</sup>    Aedah Binti Abd Rahman<sup>4</sup>    Amna Saad<sup>5</sup>

<sup>1</sup>*Department of Informatics, Universitas Trilogi, Jakarta, Indonesia*

<sup>2</sup>*Department of Agribusiness, Universitas Trilogi, Jakarta, Indonesia*

<sup>3</sup>*Department of Visual Communication Design, Universitas Trilogi, Jakarta, Indonesia*

<sup>4</sup>*Schools of Science and Technology, Asia e University, Selangor, Malaysia*

<sup>5</sup>*Malaysian Institute of Information Technology, Universiti Kuala Lumpur, Kuala Lumpur, Malaysia*

\* Corresponding author's Email: [yaddarabullah@trilogi.ac.id](mailto:yaddarabullah@trilogi.ac.id)

---

**Abstract:** This study addresses the challenge of predicting airflow volume in under-actuated zones, where occupant behavior and environmental factors complicate standard models. To improve prediction accuracy, we propose the Sigmoid Parametric Shifted ReLU (SPS-ReLU) with custom weight scaling as a novel activation function within a Multi-Layer Perceptron Artificial Neural Network (MLP-ANN) model. The model was trained and tested on a time-series dataset from a controlled environment, using optimal time intervals (5, 15, and 30 minutes) identified through polynomial regression analysis. These intervals best capture airflow patterns: the 5-minute interval effectively handles rapid fluctuations in Zones 1 and 2, while the 15-minute interval is better suited for the gradual changes in Zone 3. Results show that SPS-ReLU, particularly with a weight scale of 1.5, significantly improves accuracy, achieving an RMSE of 2.3891 and  $R^2$  of 0.9974, outperforming both standard and advanced activation functions. Comparatively, DPRReLU achieved an RMSE of 3.0469 and  $R^2$  of 0.9957, while ReLU's RMSE was 22.5458 with an  $R^2$  of 0.7741. This demonstrates SPS-ReLU's capability to balance smoothness and flexibility, enabling it to capture intricate airflow dynamics within dynamic environments. The findings highlight SPS-ReLU with custom scaling and optimal time intervals as an effective solution for enhanced airflow predictions in under-actuated zones.

**Keywords:** Airflow volume, The under-actuated zone, Neural network, Occupant behavior, Time interval, Polynomial regression, System optimization, Environmental control.

---

### 1. Introduction

Heating, Ventilation, and Air Conditioning (HVAC) systems, also referred to as building air management systems, are essential for ensuring air quality and thermal comfort in modern buildings [1]. These systems manage the regulation of airflow, temperature, and humidity across various zones, each of which may have distinct ventilation requirements [2]. HVAC systems typically function through refrigeration cycles that control the volume of airflow delivered to each zone, thereby maintaining optimal

environmental conditions [3]. The primary objective of these systems is to foster a comfortable and healthy indoor environment while balancing the needs of occupants and maximizing energy efficiency [4].

HVAC zones are generally categorized into two types: fully-actuated and under-actuated zones [5]. In fully-actuated zones, airflow volume is consistently regulated, and cooling loads are calculated based on fixed occupancy and stable environmental conditions [6]. Conversely, under-actuated zones, which feature multiple ventilation zones within a single area, exhibit more dynamic cooling loads and variable airflow demands [7]. This variability is driven

primarily by occupant behavior and the fluctuating environmental needs of different areas within the same zone. As a result, under-actuated zones pose greater challenges in maintaining proper airflow volume, due to the complexity of their ventilation requirements.

In under-actuated zones, time intervals are critical due to the cyclical nature of occupant presence and behavior, which directly impacts airflow demands across varying periods such as months, weeks, days, and specific times of day [8]. Frequent changes in occupancy require assessing airflow variations at specific intervals to meet fluctuating ventilation needs effectively. Accurate evaluation of these variations enables HVAC systems to adapt to real-time demands, ensuring consistent airflow volume for optimal thermal comfort and air quality. Conditioned air is distributed from the Air Handling Unit (AHU) machine to each zone via a network of ducts, with airflow volume regulated by Variable Air Volume (VAV) devices [7]. However, current systems rely heavily on temperature and humidity sensors with pre-configured setpoints, which are not dynamically adjusted in real time. This static approach limits the system's ability to respond to the frequent fluctuations in occupant behavior and environmental conditions within under-actuated zones, leading to inefficiencies in energy use and suboptimal air quality regulation [9]. Therefore, effective airflow control must assess specific time intervals for each zone to maintain ideal environmental conditions, considering the cyclical nature of occupancy in such variable settings.

Several studies have been conducted on the topic of airflow volume control in both fully-actuated and under-actuated zones. These studies have explored various approaches to improving indoor air quality, including occupant behavior-based ventilation using machine learning algorithms. For instance, Lee et al. [10] developed a model that optimized an Artificial Neural Network (ANN) based on mixed temperature values and the Economizer Control Algorithm, which considered both indoor and outdoor weather conditions. This model resulted in approximately 20% energy savings for HVAC systems. Similarly, Kim and Cho [8] enhanced an ANN-based model for airflow volume control, optimizing it with selected scenarios and real-time setpoint values to suit actual room conditions, leading to a 16.7% improvement in HVAC energy efficiency.

Further advancements were made by Wei et al. [11] from Beijing University took this a step further by proposing a Model Predictive Control (MPC) framework based on ANNs, which targets the airflow volume control within multi-zone VAV systems.

Their study outlined the intricate interaction between zone temperature processes and supply airflow volume control, introducing a hierarchical control approach that optimizes energy consumption. The validation through experimental data collected from a laboratory setup reinforced the potential of ANN-based MPCs in minimizing energy usage while maintaining indoor comfort. In another study, Wei et al. [12] developed an airflow volume distribution control model by optimizing ANN through offline learning using the Lagrange Variational Approach and Optimal Horizon Feedback, which resulted in a 6.12% improvement in HVAC energy efficiency.

According to previous research, the Artificial Neural Network (ANN) approach is the most often used method for airflow volume prediction-based occupant behavior. This machine learning technique excels at modelling non-linear relationships and has proven effective in capturing the complex dynamics of occupancy-driven airflow. However, the performance of ANN models largely depends on the choice of activation function [13], which can significantly affect their ability to handle varying environmental conditions, especially in cyclical patterns across different zones. Proper weight initialization can significantly enhance the model's convergence and stability, further improving predictive accuracy [14].

Standard activation functions such as ReLU (Rectified Linear Unit), PReLU (Parametric ReLU), and Leaky ReLU are widely used for their simplicity and computational efficiency. ReLU is particularly popular for addressing vanishing gradient issues, but in complex environments with varying occupancy across multiple zones, it can result in lower smoothness scores, limited output range, and higher final training loss, affecting its ability to accurately predict cyclical airflow patterns [15]. PReLU and Leaky ReLU, by incorporating small negative slopes, offer an extended output range and improved smoothness scores, contributing to lower final training loss [16, 17]. However, despite these enhancements, both PReLU and Leaky ReLU still face challenges in fully adapting to dynamic environments with fluctuating occupant behavior, especially when predicting cyclical airflow variations in real-time.

To address the limitations of standard activation functions, more advanced functions such as Flexible Rectified Linear Units (FReLU) and Dynamic Parametric Rectified Linear Units (DPRReLU) have been developed. FReLU introduces flexibility by allowing the activation threshold to be learned, enhancing model adaptability across varying environmental conditions and zones [18]. However,

this added complexity can result in overfitting, especially in small datasets or highly variable occupancy scenarios. DPreLU incorporates dynamic parameters that adjust based on input features, making it more suitable for environments with fluctuating occupancy and cyclical patterns [19]. Despite these improvements, DPreLU's increased model complexity can lead to higher computational demands and increased complexity due to more learnable parameters. While both FReLU and DPreLU improve the handling of dynamic airflow demands and occupancy variations, challenges remain in fully optimizing ANN models for airflow volume prediction across different zones, particularly in cyclical behaviors and real-time fluctuations. Therefore, further refinement of activation functions is essential to enhance accuracy and efficiency of airflow volume prediction.

In addition to the choice of activation function, the issue of weight initialization is crucial to the performance of an ANN model [20]. Improper weight initialization can lead to vanishing or exploding gradients, which can hinder the model's learning process during backpropagation [21]. If the weights are too small, the gradients may shrink exponentially, causing slow learning or even stopping the training [22]. On the other hand, if the weights are too large, the gradients can grow uncontrollably, leading to unstable updates and divergence during training. In environments with cyclical patterns and fluctuating conditions such as varying airflow across different zones due to occupant behavior careful weight initialization is crucial [23]. Standard methods like Glorot (Xavier) and He initialization promote stable gradient flow, but they have limitations. Glorot assumes symmetrical activations and normalized inputs, which may not hold in complex, non-linear models, leading to underfitting [24]. He initialization works well with ReLU but may not handle cyclical patterns effectively [25]. Both methods can fail to capture subtle environmental variations, risking underfitting or overfitting. To improve model generalization, customized initialization strategies, such as scaled initializations was needed to better adapt to the dynamic relationships between occupant behavior and airflow.

The present study proposes an advanced airflow volume prediction model using a Multilayer Perceptron Artificial Neural Network (MLP-ANN) with a novel Sigmoid Parametric Shifted ReLU (SPS-ReLU) activation function. This proposed model incorporates strong improvements in predictive performance through three primary strengths: the unique combination of the sigmoid and ReLU functions in SPS-ReLU, which offers dynamic

adaptability to both positive and negative input values for better handling of non-linear patterns; a custom weight scaling method for precise control over neuron activation, which improves model convergence and accuracy in complex, cyclical environments; and an optimized feature engineering process that captures spatial, temporal, and behavioral variations crucial for reliable predictions in under-actuated zones. Together, these elements create a robust model that effectively balances predictive accuracy, smoothness, and computational efficiency, improving the ability of HVAC systems to manage airflow volume in dynamic, occupant-driven settings.

The organization of this research paper adheres to a structured approach, beginning with a comprehensive introduction to the proposed Sigmoid Parametric Shifted ReLU (SPS-ReLU) activation function and its significance in airflow volume prediction within under-actuated zones. We then explore the theoretical foundations of activation functions and custom weight scaling methods, providing the rationale for incorporating SPS-ReLU within a Multilayer Perceptron Artificial Neural Network (MLP-ANN) framework. Subsequently, we meticulously outline our methodology, detailing the data collection process, feature engineering techniques, and model architecture design, all tailored to enhance predictive performance in dynamic, occupant-driven environments. The empirical analysis section presents an in-depth evaluation of experimental results, comparing the SPS-ReLU activation function against both standard and advanced activation functions in terms of predictive accuracy and generalization. Finally, we conclude with a thorough discussion and interpretation of the findings, highlighting the implications of SPS-ReLU in enhancing HVAC system efficiency and proposing potential directions for future research in predictive modeling for airflow control in under-actuated zones.

## 2. Methods

This case study was executed at the Universitas Trilogi Library, as illustrated in Fig. 1. The library comprised five rooms, designated from 1 to 7, which constituted the under-actuated zones. Each zone encompassed multiple distinct areas. Data collection and observational sampling were systematically undertaken in room 3, specifically within a corner section. This room was segmented into three ventilation-specific areas, each with a coverage of 25 m<sup>2</sup>, providing a structured environment for the

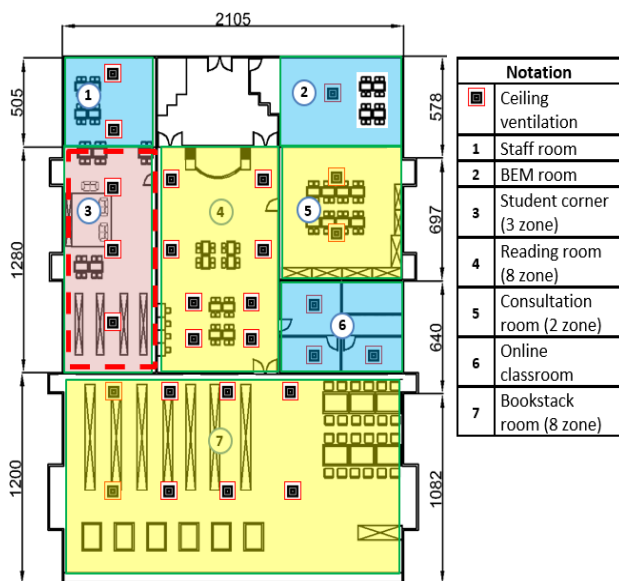


Figure . 1 Layout of Universitas Trilogi Library

analysis of occupant behavior and environmental conditions.

This research employed a systematic methodology, starting with data collection in the Universitas Trilogi Library, specifically focusing on room 4, which was divided into three ventilation-specific areas of 25 m<sup>2</sup> each. Airflow volume was measured in these areas to capture real-time dynamics, while time intervals were set at 5, 15, 30, and 60 minutes to track fluctuations in occupant behavior and environmental conditions. The pre-processing stage involved feature engineering to create new variables, followed by feature selection and retention to refine the dataset for optimal performance. A predictive model for airflow volume was developed using a Multilayer Perceptron Artificial Neural Network (MLP-ANN) with optimized activation functions. The model's performance was rigorously assessed through Root Mean Squared Error (RMSE), R<sup>2</sup>, and comparative evaluations of various activation functions. In the final stage, the proposed model, incorporating SPS-ReLU with custom weight initialization, was compared against state-of-the-art ANN models using standard activation functions (ReLU, PReLU, Leaky ReLU) and advanced functions (FReLU and DPRELU), demonstrating its improved performance.

### 2.1. Data collections

Data for this research were systematically gathered from three distinct zones (Zone 1, Zone 2, and Zone 3) within an office environment during regular weekdays (Monday to Friday) from 8 AM to 4 PM. Spanning a total of 14 weeks, the data collection covered several weeks of continuous

observation. Throughout this period, observations were recorded at 5-minute intervals, resulting in a comprehensive dataset that captured detailed insights into the occupant dynamics and environmental conditions. A total of 478 individuals were observed during the entire duration, with the data meticulously covering a range of occupant activities including sitting, standing, walking, reading, talking, squatting, writing, sleeping, typing, and the use of electronic devices such as headphones, laptops, and mobile phones.

The data related to occupant behavior was manually recorded by reviewing CCTV footage, and the frequency and number of occupants engaging in each activity were documented. This information was organized into a spreadsheet, with each variable representing a distinct occupant activity. Simultaneously, indoor and outdoor environmental conditions, including temperature, relative humidity, and air pressure, were collected automatically using sensors installed in each zone. These sensor data were extracted and saved in separate spreadsheet files. Finally, the occupant behavior data and environmental data were integrated into a single unified dataset, allowing for a holistic analysis of the relationship between occupancy patterns and environmental factors.

### 2.2. Airflow volume measurement

Accurate measurement of airflow volume is essential in maintaining optimal environmental conditions within HVAC systems, particularly in under-actuated zones where occupant behavior and environmental variables fluctuate dynamically. In this study, airflow volume was determined through a series of calculations that account for initial airflow requirements, air needed per person, and ventilation air [26]. These calculations provide a comprehensive measure of airflow distribution to meet both occupant and environmental demands. The formula for calculating the total airflow volume is as follows:

$$AV_2 = AV_1 + ARP + VA \tag{1}$$

Where:

- AV<sub>2</sub> represents the total airflow volume,
- AV<sub>1</sub> is the initial airflow volume,
- ARP is the air required per person, and
- VA denotes the ventilation air.

The initial airflow volume (AV<sub>1</sub>) is determined by three primary factors: the airflow requirement for the area's size, the rate of air exchange, and the minimum airflow per occupant. It is calculated as follows:

$$AV_1 = CFM_{area} + CFM_{change} + \min CFM_{person} \quad (2)$$

Where:

- $CFM_{area}$  is the airflow requirement based on the area’s volume,
- $CFM_{change}$  indicates the rate of air exchange per minute (set to 8.3 cubic meters per minute in this study), and
- $CFM_{person}$  is the minimum airflow volume required per person (typically set to 20 CFM).

This calculation ensures that each area has a sufficient baseline airflow volume based on its size, ventilation rate, and the presence of occupants.

Ventilation air (VA) is calculated to maintain proper indoor air quality by considering the difference in humidity levels between indoor and outdoor environments [27]. This can be mathematically expressed as:

$$VA = \frac{Q_{total}}{4340 \times (Hum_{out} - Hum_{in})} \quad (3)$$

Where:

- $Q_{total}$  represents the total airflow volume,
- $Hum_{out}$  is the humidity level outside the building, and
- $Hum_{in}$  is the humidity level inside the building.

This formula accounts for the added ventilation air required to balance indoor humidity, particularly when there are significant differences between indoor and outdoor humidity levels, which can affect occupant comfort and indoor air quality.

### 2.3. Time interval measurement

In this section, 3rd-degree polynomial regression was employed to assess the relationship between airflow volume and different time intervals [28] (5 minutes, 15 minutes, 30 minutes, and 60 minutes) for each of the three zones (Zone 1, Zone 2, and Zone 3). The purpose of this analysis was to determine the most appropriate time interval for capturing fluctuations in airflow volume by evaluating the  $R^2$  values, which represent the goodness of fit of the polynomial model. The general form of a 3rd-degree polynomial regression is expressed as:

$$y = \beta_0 + \beta_1x + \beta_2x^2 + \beta_3x^3 \quad (4)$$

Where:

- $y$  represents the predicted value,
- $x$  denotes the time interval (in minutes),
- $\beta_0$  is the intercept,
- $\beta_1, \beta_2, \beta_3$  are the coefficients

corresponding to the linear, quadratic, and cubic terms, respectively.

This mathematical formulation allows the model to capture nonlinear relationships between time intervals and airflow volume, accounting for the complexity of airflow volume changes over different time periods in each zone.

### 2.4. Feature pre-processing

This step includes feature engineering, feature selection, and feature retention. Feature engineering is a critical first step in predictive modelling, aimed at transforming raw data into meaningful input that can enhance the model’s performance.

#### 1. Feature Engineering

To capture the repetitive daily patterns inherent in the time variable, cyclic encoding of time was performed. Time, which repeats every 24 hours, was transformed into two cyclic components using sine and cosine functions. The transformation ensures that the model can recognize the cyclical nature of time, avoiding discontinuities between the end and start of the day [29, 30]. The formulas for time encoding are:

$$time_{cos} = \cos\left(\frac{2\pi \times time_{in\_minutes}}{1440}\right) \quad (5)$$

$$time_{sin} = \sin\left(\frac{2\pi \times time_{in\_minutes}}{1440}\right) \quad (6)$$

Where time represents the hour of the day, ranging from 0 to 23. These transformations enable the model to detect cyclic patterns over time, which is crucial for data exhibiting strong daily or seasonal variations.

Additionally, the zone feature was one-hot encoded to account for the spatial variation in air volume requirements across different zones. One-hot encoding involves converting categorical variables into binary vectors [31]. For example, if the dataset has three zones (zone\_1, zone\_2, zone\_3), each zone is represented as a binary feature. This allows the model to treat each zone distinctly, ensuring that the spatial characteristics of each zone are preserved in the dataset.

#### 2. Feature Selection

The next critical task was to identify which of these features had the most significant impact on the target variable air volume. To achieve this, the study employed mutual information regression, a robust non-linear method for measuring the dependency between the input features and the target. Mutual information is especially suited for this study as it captures both linear and non-linear relationships, which are likely to exist in such a complex

environment influenced by dynamic factors like temperature, humidity, and human occupancy. Mutual information is defined as the reduction in uncertainty of the one variable given knowledge of another [32]. For two random variables X (a feature) and Y (the target variable), mutual information  $I(X;Y)$  is computed as:

$$I(X;Y) = \sum_{x \in X} \sum_{y \in Y} p(x,y) \log \left( \frac{p(x,y)}{p(x)p(y)} \right) \quad (7)$$

Where:

- $p(x,y)$  is the joint probability distribution of X and Y,
- $p(x)$  and  $p(y)$  are the marginal probabilities of X and Y, respectively.

In this study, features with mutual information scores above a threshold of 0.5 were retained for their high predictive power, while those below the threshold were excluded to streamline the model.

Table 1. Dataset Features

Features	Description
num-occupant	The total number of occupants present in the zone.
num-stand	The number of occupants standing in the zone.
num-sit	The number of occupants sitting in the zone.
num-walk	The number of occupants walking in the zone.
num-squat	The number of occupants squatting in the zone.
num-read	The number of occupants reading in the zone.
num-talk	The number of occupants talking in the zone.
num-write	The number of occupants writing in the zone.
num-sleep	The number of occupants sleeping in the zone.
num-typing	The number of occupants typing in the zone.
num-light- work	The number of occupants engaged in light work in the zone.
num- headphone	The number of occupants using headphones in the zone.
num- mobilephone	The number of occupants using mobile phones in the zone.
num-computer	The number of occupants using computers in the zone.
indoor-temp	The temperature inside the monitored zone
indoor-hum	The relative humidity inside the monitored zone (in %).
indoor-air- pressure	The air pressure inside the monitored zone (in Pa).
outdoor-temp	The temperature outside the monitored zone
outdoor-hum	The relative humidity outside the monitored zone (in %).
outdoor-air- pressure	The air pressure outside the monitored zone
cfm-vent-air	The volume of air being supplied to the zone by the ventilation system, measured in cubic feet per minute (CFM)
time-sin	The sine transformation of the time in minutes to reflect cyclical patterns (e.g., daily cycles).
time-cos	The cosine transformation of the time in minutes to complement the sine representation.
zone one-hot	One-hot encoded representation of the zones, where each zone is represented by a binary feature: zone_1, zone_2, and zone_3, indicating whether the observation belongs to that specific
air-vol-req	The required volume of air to meet the environmental and occupant demands in the zone

### 3. Feature Retention

One of the challenges identified in the feature selection process was the risk of eliminating features that, despite having low mutual information scores, were known to be contextually important specifically, time and zone. Feature retention was employed to address this issue. In this phase, the engineered features for time (time\_sin, time\_cos) and the one-hot encoded zones were force-retained in the final feature set. This approach aligns with the understanding that feature selection is not merely about statistical significance but also about contextual relevance, which can enhance model performance and interpretability [33, 34].

This decision was rooted in the understanding that these features, while possibly showing lower statistical relevance in mutual information, are indispensable for maintaining the model’s connection to real-world temporal and spatial contexts. Retaining these features ensures that the model reflects the operational realities of air volume dynamics, which vary based on both the time of day and the specific zone being observed.

The retained features, in combination with the high-ranking features from mutual information, form a comprehensive set that balances statistical importance with domain-specific knowledge. This holistic feature selection and retention strategy safeguards against the loss of critical contextual variables, thereby enhancing the model's capacity to make reliable predictions across varying temporal and spatial conditions.

### 2.5. Dataset features

The dataset is a comprehensive combination of feature engineered and original features, encompassing occupant behavior, electronic usage, and environmental conditions. These features have been meticulously curated to capture the complexities of the airflow system in under-actuated zones. The target variable, or output feature, is airflow volume, which is essential for assessing the efficiency and accuracy of predictive models within the study. Table 1 presents a detailed breakdown of the dataset's features, which are instrumental in examining both the environmental and occupant-driven factors that influence airflow dynamics. By integrating cyclic time transformations and zone-specific one-hot encodings, the dataset offers a robust structure for understanding the interplay between time, occupancy, and environmental conditions in predicting airflow volume.

### 2.6. Airflow volume prediction mode

In this study, a Multilayer Perceptron Artificial Neural Network (MLP-ANN) was developed to predict airflow volume requirements in under-actuated zones, with a focus on optimizing the model through hyperparameter tuning. The architecture of the MLP-ANN consisted of three primary layers: 1 input layer, 1 hidden layer, and 1 output layer, each playing a critical role in transforming the input data into accurate airflow volume predictions. The experiment was conducted across three distinct models based on the activation functions used. The First Model employed standard activation functions [35], including ReLU, PReLU, and Leaky ReLU. The Second Model utilized more advanced activation functions, such as FReLU [18] and DPRELU [19]. Finally, the Third Model implemented the proposed approach, featuring a Sigmoid Parametric Shift ReLU (SPS-ReLU) with a custom scale of weight initialization.

The hyperparameters for all models were carefully selected to balance computational efficiency and model performance in learning complex patterns. Below is a Table 2 outlining the hyperparameter tuning strategies:

The number of neurons in the first hidden layer was varied within a range of 32 to 128, optimizing both the learning capacity and computational load. To mitigate overfitting, a dropout rate between 0.0 and 2.0 was employed, deactivating neurons during training to improve the model's generalization ability. The learning rate was adjusted between  $1 \times 10^{-4}$  and  $1 \times 10^{-2}$ , ensuring effective gradient updates during optimization. All models used a batch size of 32 and were trained for 100 epochs, providing sufficient iterations for convergence.

Hyperparameter tuning was performed using the Random Search technique with 50 iterations, which efficiently explored the hyperparameter space without the need for exhaustive searches. The Adam

Table 2. Hyperparameter Strategies

Hyperparameter	Range
Neurons in hidden layer	32 to 128
Dropout rate	0.0 to 2.0
Learning rate	$1 \times 10^{-4}$ to $1 \times 10^{-2}$
Batch size	32
Epochs	100
Optimizer	Adam
Random search iterations	50
Cross-validation	10-Fold

optimizer, known for its adaptive learning rates and efficiency in deep learning tasks, was used for model training. To evaluate model robustness and generalization, a 10-fold cross-validation was applied, dividing the dataset into multiple training and validation subsets to ensure a comprehensive performance evaluation.

## 2.7. Proposed method of activation function

The Proposed Model, however, introduced the novel Sigmoid Parametric Shifted ReLU (SPS-ReLU), which combines the strengths of the sigmoid and ReLU functions. SPS-ReLU incorporates a trainable shift parameter  $\beta$ , allowing the function to dynamically adjust neuron activations based on input values, making it particularly well-suited to capturing the nonlinearities in airflow volume predictions. The SPS-ReLU function is mathematically expressed as:

$$f(x) = \begin{cases} \alpha(\sigma(x - \beta)), & \text{if } x < \beta \\ \alpha(x - \beta), & \text{if } x \geq \beta \end{cases} \quad (8)$$

Where  $\alpha$  is a scaling parameter,  $\beta$  is a shift parameter, and  $\sigma(x)$  is the sigmoid function. This novel function smooths transitions and prevents abrupt neuron deactivation, enhancing the model's ability to learn from complex, nonlinear data patterns.

## 2.8. Custom scale of weight initialization

A custom weight initialization method was developed, grounded in the principles of Glorot Uniform initialization, to enhance the neural network model's performance. This custom initializer introduced an adjustable scale parameter, allowing for the fine-tuning of the weight initialization range to better accommodate the specific architecture of the model. The initializer was implemented by constructing a class that extends `tf.keras.initializers.Initializer`, enabling precise control over the initialization process. The computation of the limit for the uniform distribution was adapted from the Glorot Uniform formula, with the number of input units (`fan_in`) and output units (`fan_out`) derived from the weight tensor's shape. The scale parameter introduces enhanced flexibility, enabling more precise control over the weight initialization range. The limit is calculated as:

$$\text{limit} = \text{scale} \times \sqrt{\frac{6.0}{\text{fan}_{in} + \text{fan}_{out}}} \quad (9)$$

By adjusting the scale, it becomes possible to better regulate the distribution of weights across the

neural network. The boundaries for weight initialization are determined by this scale, which defines the limit within which the weights are drawn. Mathematically, the weights are sampled from a uniform distribution that lies within the interval specified by the computed limit. Mathematically, this can be expressed as:

$$W \sim \text{Uniform}(-\text{limit}, \text{limit}) \quad (10)$$

The weight matrix, denoted as  $W$ , is initialized using a limit that is computed based on the scale parameter. This approach guarantees that the weights are uniformly distributed within the range  $[-\text{limit}, \text{limit}]$ , ensuring balanced initialization. By constraining the weights within this interval, the method promotes faster convergence and enhances the efficiency of model training, ultimately leading to improved performance and stability during the learning process.

## 2.9. Model evaluation

The evaluation of the MLP-ANN prediction model's performance was carried out using three key metrics: Root Mean Squared Error (RMSE), Mean and the coefficient of determination ( $R^2$ ). RMSE, widely used for measuring prediction errors [36], represents the average magnitude of those errors and is defined mathematically as:

$$\text{RMSE} = \sqrt{\frac{1}{n} \sum_{t=1}^n (A_t - F_t)^2} \quad (11)$$

$R^2$ , known as the coefficient of determination, is a critical metric used to assess the extent to which the variance in the target variable is explained by the input features of the model [37].  $R^2$  values range from 0 to 1, where a value approaching 1 reflects a higher level of predictive accuracy. Essentially, a higher  $R^2$  suggests that the model provides a superior fit to the observed data. The formula for computing  $R^2$  is as follows:

$$R^2 = 1 - \frac{\sum_{i=1}^n (y_i - \hat{y}_i)^2}{\sum_{i=1}^n (y_i - \bar{y}_i)^2} \quad (12)$$

## 2.10. Activation function evaluation

The activation function evaluation of the MLP-ANN prediction model's performance was carried out using four key metrics: smoothness score and final training loss. The smoothness score of an activation function quantifies the extent to which the function

generates continuous and differentiable outputs [38]. This smoothness can be measured either by analyzing the second derivative of the activation function or by assessing the variance of gradients throughout the training process. Mathematically, the smoothness score, denoted as  $S$ , can be estimated as follows:

$$S = \frac{1}{N} \sum_{i=1}^N \left| \frac{\partial^2 f(x_i)}{\partial x^2} \right| \quad (13)$$

In this context,  $f(x_i)$  denotes the activation function applied to the input  $x_i$ , while  $N$  represents the total number of inputs. A lower smoothness score,  $S$ , signifies a smoother activation function. For practical evaluation, the smoothness of the function can be empirically assessed by monitoring the variance of the gradients during training.

Table 3. Nomenclature for the Methods Section

Symbol	Description	Units
$AV_2$	Total airflow volume required for the area	CFM (cubic feet per minute)
$AV_1$	Initial or baseline airflow volume for the area	CFM
ARP	Airflow volume required per occupant	CFM
VA	Ventilation air required based on humidity levels	CFM
$CFM_{area}$	Airflow requirement based on area volume	CFM
$CFM_{change}$	Rate of air exchange per minute for the area	CFM
$CFM_{min}$	Minimum airflow volume required per occupant	CFM
$Q_{total}$	Total initial airflow volume without humidity adjustment	CFM
$Hum_{out}$	Humidity level outside the building	% (percentage)
$Hum_{in}$	Humidity level inside the building	% (percentage)
time_sin	Sine transformation of the time variable to reflect daily cyclic patterns	-
time_cos	Cosine transformation of the time variable to reflect daily cyclic patterns	-
$I(X; Y)$	Mutual information between a feature $X$ and the target variable $Y$	-
$p(x, y)$	Joint probability distribution of variables $X$ and $Y$	Probability
$p(x)$	Marginal probability of $X$	Probability
$p(y)$	Marginal probability of $Y$	Probability
$x$	Time interval (in minutes)	Minutes
$\beta_0$	Intercept in the polynomial regression	-
$\beta_1, \beta_2, \beta_3$	Coefficients for the linear, quadratic, and cubic terms in polynomial regression	-
$y$	Predicted value in the polynomial regression	-
$S$	Smoothness score of an activation function, measuring continuity and differentiability	-
$f(x_i)$	Activation function applied to input $x_i$	-
$N$	Total number of inputs or samples	-
$L$	Training loss, often computed as Mean Squared Error (MSE) in regression tasks	-
$y_i$	Actual value in training loss calculation	-
$\hat{y}_i$	Predicted value in training loss calculation	-
$W$	Weight matrix in neural network initialization	-
$\alpha$	Scaling parameter in SPS-ReLU activation function	-
$B$	Shift parameter in SPS-ReLU activation function	-
$\sigma(x)$	Sigmoid function applied to input $x$	-

The final training loss serves as a critical measure of how effectively the neural network has learned from the training data [39]. It quantifies the difference between the network's predictions and the actual values, where lower loss values indicate superior performance. Depending on the specific task, various loss functions can be employed to calculate the training loss,  $L$ . For regression tasks, the mean squared error (MSE) is often the preferred choice and can be calculated as follows:

$$L_{\text{MSE}} = \frac{1}{N} \sum_{i=1}^N (y_i - \hat{y}_i)^2 \quad (14)$$

In this formula,  $y_i$  represents the actual value, while  $\hat{y}_i$  corresponds to the predicted value.  $N$  denotes the total number of samples.

### 2.11. Nomenclature

Table 3 present definitions for all variables, symbols, and terms used in the mathematical formulations throughout the Methods section. Each entry includes the symbol, a description of its role in the calculations, and the relevant units to aid in understanding the technical components of the airflow volume prediction model.

## 3. Result and discussion

The experiments were conducted using Python with the TensorFlow and Keras frameworks, leveraging their built-in functionalities to implement the proposed SPS-ReLU activation function and track key performance metrics. Each model, including the MLP-ANN models with standard activation functions (ReLU, PReLU, Leaky ReLU) [35] and advanced activation functions includes FReLU [18] and DPreLU [19], as well as the state-of-the-art methods, was trained over a series of epochs until convergence. Performance metrics such as RMSE,  $R^2$ , smoothness score, and final training loss were logged at each epoch to monitor the learning progression. Cross-validation was performed to evaluate the generalizability of each activation function across different subsets of the dataset, thereby mitigating the risk of overfitting.

### 3.1. Proper time interval

Table 4 presents the results of the polynomial regression analysis across four different time intervals (5, 15, 30, and 60 minutes), demonstrating varying degrees of efficacy in capturing airflow volume patterns across the three zones.

Table 4.  $R^2$  Score Comparison of Different Time Intervals for Each Zone

Time Intervals	$R^2$ Score		
	Zone 1	Zone 2	Zone 3
5 min	0,044	0,061	0,015
15 min	0,043	0,059	0,019
30 min	0,030	0,019	0,012
60 min	0,010	0,011	0,010

For Zone 1, the 5-minute interval demonstrated superior performance, achieving the highest  $R^2$  value (0.044). This indicates that the model effectively captured intricate and rapid variations in airflow volume, which are primarily modulated by real-time occupant behavior and dynamically fluctuating environmental factors. The finer granularity afforded by this interval enabled a more precise representation of immediate changes, thereby enhancing the model's sensitivity to subtle, short-term variations. In Zone 2, the 5-minute interval similarly yielded the highest  $R^2$  value (0.061), underscoring its efficacy in harmonizing short-term volatility with longer-term trends. This interval provided an optimal framework for zones experiencing moderate airflow changes, allowing the model to encompass both transient shifts and gradual variations, thereby offering a comprehensive solution for processing temporally-sensitive data.

Conversely, Zone 3 exhibited its best performance with the 15-minute interval, achieving a marginally higher  $R^2$  value (0.019) than the 5-minute interval. This interval proved more adept at modelling slower, non-linear airflow volume patterns, particularly in this zone, where changes tend to unfold over longer periods. The inclusion of cubic terms in the 3rd-degree polynomial model provided a more sophisticated representation of the gradual and complex airflow dynamics prevalent in this area. While the 60-minute interval was tested across all zones, it generally resulted in lower  $R^2$  values, suggesting it is less effective at capturing more frequent and immediate airflow volume variations, particularly in zones with high occupant activity fluctuations.

### 3.2. Feature pre-processing

The feature selection process, conducted post-feature engineering, has culminated in a strategically refined set of variables crucial for accurately predicting airflow volume within under-actuated zones. This selection was informed by the Mutual Information Scores, as depicted in the correlation heatmap (Fig. 2), which provides an analytical

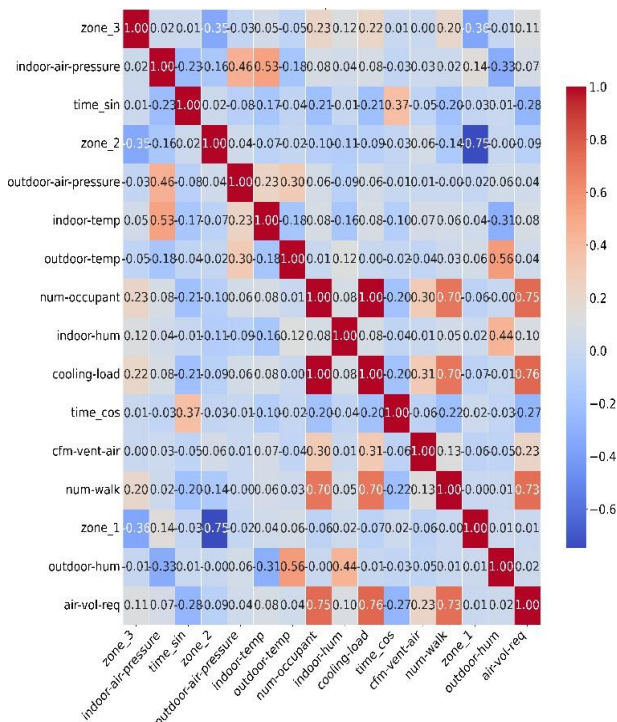


Figure. 2 Correlation Heatmap of Selected Features

visualization of the interrelationships among the key features in the dataset.

The process involved a sophisticated evaluation of feature relevance, allowing for a more targeted and efficient predictive model by isolating the variables most influential in capturing the dynamics of airflow volume. The heatmap highlights the pivotal role of features such as cfm-vent-air (1.905), cooling-load (1.737), and num-occupant (1.636), which emerged as the most influential predictors in modeling airflow volume. These features capture the fundamental dynamics of the HVAC system, particularly the interplay between ventilation rates, thermal load, and occupant density, which are critical for predicting airflow patterns across different zones. The integration of environmental variables, including outdoor-hum (0.782), outdoor-air-pressure (0.764), and indoor-air-pressure (0.583), underscores the significance of both external and internal climatic conditions in modulating airflow.

As demonstrated in Fig. 2, these environmental factors show moderate correlations with airflow volume and cooling load, underscoring their role in predicting system responses to evolving atmospheric conditions. Their inclusion ensures the model captures the influence of environmental fluctuations, particularly in zones where such variations are pronounced. Additionally, time-based features such as time\_sin (0.085) and time\_cos (0.052) were retained for their capacity to represent periodic fluctuations in occupant behavior and environmental

Table 5. Top Selected Features Based on Mutual Information Score

Features	Mutual Information Score
cfm-vent-air	1.905
cooling-load	1.737
num-occupant	1.636
num-walk	0.832
outdoor-hum	0.782
outdoor-air-pressure	0.764
outdoor-temp	0.734
indoor-hum	0.625
indoor-temp	0.586
indoor-air-pressure	0.583
outdoor-air-pressure	0.764
outdoor-temp	0.734
indoor-hum	0.625
indoor-temp	0.586
indoor-air-pressure	0.583

conditions, reflecting cyclical patterns over the day. These features are crucial for accounting for temporal shifts, as evidenced by their correlation with num-walk (0.832), a significant predictor of airflow variability.

The cyclic encoding of time enables the model to capture both immediate changes and long-term trends in airflow dynamics. Furthermore, zone-specific variables, zone\_1 (0.058), zone\_2 (0.056), and zone\_3 (0.042), were preserved to address spatial variability across zones. These one-hot encoded features allow the model to adjust its predictions based on the unique characteristics of each zone, thus improving its predictive accuracy across distinct spatial contexts.

The final set of selected features, summarized in Table 5, represents a comprehensive framework for predicting airflow volume. It strikes a balance between occupant behavior, environmental conditions, and temporal patterns, providing a solid foundation for a model that is both responsive to real-time fluctuations and capable of capturing long-term trends.

### 3.3. Airflow volume prediction model

The hyperparameter tuning results, as detailed in Table 6, reveal the optimal configurations identified for each activation function within the MLP-ANN model. Key parameters, such as the number of units, dropout rate, learning rate, and, where applicable, the alpha and beta values, were meticulously optimized to maximize the model’s predictive capabilities. This

fine-tuning process encompassed a range of activation functions, including standard activation function [35] like ReLU, PReLU, and Leaky ReLU, as well as more advanced functions such as FReLU [18] and DPRELU [19]. Additionally, the Sigmoid Parametric Shifted ReLU (SPS-ReLU) with custom weight scales (0.5, 1.0, 1.5, 2.0) was calibrated to further enhance model performance. These adjustments reflect a targeted approach to refining the model’s architecture, ensuring that each activation function is optimally configured to handle the complexity of the predictive task.

The ReLU activation function reached its optimal setup with 320 units, a dropout rate of 0.2, and a 0.01 learning rate, indicating that this balanced configuration reduces overfitting while maintaining efficient learning. PReLU and Leaky ReLU, which process negative input values differently, required larger networks with 384 and 480 units respectively, along with similar dropout and learning rates,

Table 6. Hyperparameter Tuning Results for the MLP-ANN Model Across Different Activation Functions

Activation Function	Units	Dropout Rate	Learning Rate
ReLU [35]	320	0.2	0.01
PReLU [35]	384	0.2	0.01
Leaky ReLU [35]	480	0.2	0.01
FReLU [18]	512	0.3	0.01
DPReLU [19]	352	0.2	0.01
SPS-ReLU scale 0.5	64	0.2	0.004
SPS-ReLU scale 1.0	96	0.1	0.001
SPS-ReLU scale 1.5	96	0.1	0.002
SPS-ReLU scale 2.0	128	0.1	0.002

highlighting their need for greater capacity to capture intricate patterns. FReLU performed best with 512 units and a 0.3 dropout rate, reflecting its ability to handle complex nonlinearities but with higher regularization. DPRELU, another advanced

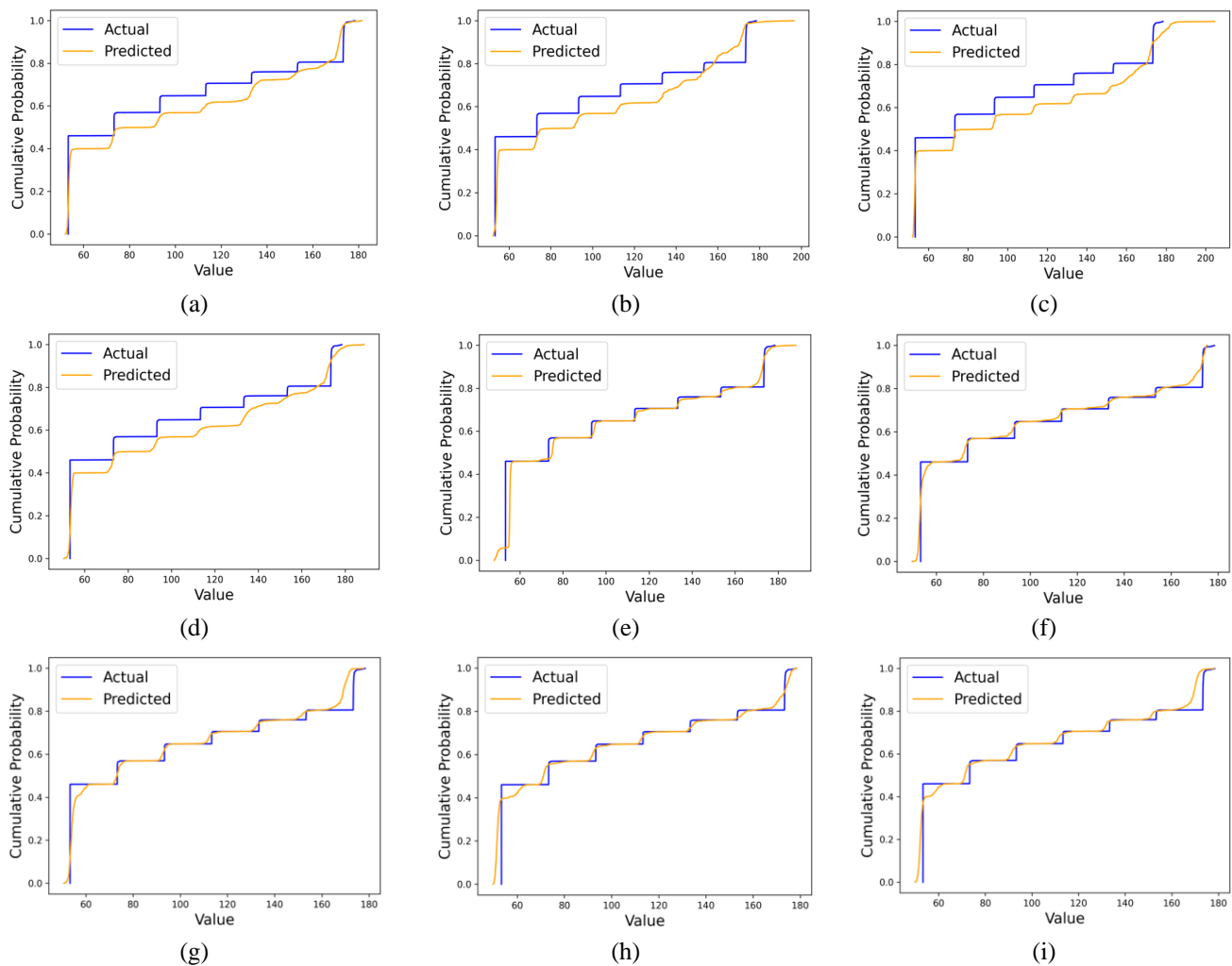


Figure. 3 CDF Plot of Models Across Different Activation Function: (a) ReLU, (b) PReLU, (c) Leaky ReLU, (d) FReLU, (e) DPRELU, (f) SPS-ReLU scale 0.5, (g) SPS-ReLU scale 1.0, (h) SPS-ReLU scale 1.5, and (i) SPS-ReLU scale 2.0

activation, found balance at 352 units and moderate regularization. The Sigmoid Parametric Shifted ReLU (SPS-ReLU), utilizing custom weight scales, adapted its configurations accordingly. For lower scales (0.5), it required fewer units (64) and a learning rate of 0.004. As the scale increased (1.0 to 2.0), the model demanded more units, with the best setup at 128 units and a 0.002 learning rate for a 2.0 weight scale. This flexibility suggests that SPS-ReLU adjusts effectively to different input scales, requiring careful tuning of units and learning rates to optimize performance.

The CDF (Cumulative Distribution Function) plots in Fig. 3 present the results of airflow volume prediction using various activation functions implemented in an MLP-ANN model. These graphs demonstrate the alignment between actual and predicted values, enabling a comprehensive evaluation of model performance across different activation functions.

Beginning with ReLU (Fig. 3 (a)), the plot shows a clear deviation between actual and predicted values. While it captures the overall trend, the model struggles with finer details, leading to less accurate predictions. This suggests that ReLU's inability to handle negative values may result in information loss, particularly in under-actuated zones. In contrast, PReLU (Fig. 3 (b)) shows improved alignment, as its learnable parameters adjust for negative inputs, narrowing the gap between actual and predicted values. Leaky ReLU (Fig. 3 (c)) further enhances prediction consistency by incorporating a small slope for negative inputs, offering smoother alignment and better accuracy across a broader range of airflow dynamics.

The FReLU (Fig. 3 (d)) and DPRELU (Fig. 3 (f)) activation functions also display reasonably accurate predictions, closely following the actual cumulative probability trends. These functions' adaptations emphasize their flexibility in managing both positive and negative inputs, allowing them to generalize better across diverse airflow volume conditions.

The SPS-ReLU with scaling factors (Figs. 3 (g)–(j)) showcases progressive improvements in predictive performance as the scale increases. While the model with a scale of 0.5 (Fig. 3 (g)) shows moderate performance, the predictions become increasingly aligned with actual values as the scale reaches 2.0 (Fig. 3 (j)). This scaling amplifies the model's sensitivity to airflow volume variations, suggesting that higher scaling factors in SPS-ReLU enhance model adaptability, improving its generalization and prediction accuracy in complex under-actuated zones.

### 3.4. Model performance

The model performance evaluation, as depicted in Table 7, provides insightful distinctions among the activation functions in terms of predictive accuracy and generalization ability for airflow volume prediction within under-actuated zones. By analyzing the Root Mean Square Error (RMSE) and  $R^2$  metrics, we can infer the strengths and limitations of each activation function in capturing complex airflow dynamics.

Starting with ReLU, the model yields an RMSE of 22.5458 and an  $R^2$  of 0.7741, indicating moderate predictive performance. Despite its simplicity, ReLU struggles to model the inherent non-linearity of airflow volume accurately, as evidenced by a relatively high error and lower  $R^2$  value. This suggests that ReLU's inability to activate negative values might result in the underestimation of certain patterns in airflow dynamics.

The PReLU function, with an RMSE of 23.7645 and  $R^2$  of 0.7489, performs slightly worse than ReLU, which may be attributed to overfitting or an ineffective adaptation of the learnable parameters in this context. The increase in RMSE and corresponding decrease in  $R^2$  suggest that the model does not generalize as effectively when leveraging the flexibility of PReLU. Leaky ReLU, with a significant increase in RMSE to 30.0834 and an  $R^2$  of 0.5979, exhibits the lowest performance among the functions tested. This performance degradation highlights that the model, even with a small slope for negative values, fails to capture the airflow volume patterns adequately. The high error and poor fit (low  $R^2$ ) suggest that Leaky ReLU introduces excessive noise into the model, compromising its prediction capabilities.

FReLU offers an improvement over Leaky ReLU and PReLU, with an RMSE of 23.1021 and  $R^2$  of 0.7623, positioning it closer to ReLU's performance.

Table 7. Model Performance Based Activation Functions

Activation Function	RMSE	$R^2$
ReLU [35]	22.5458	0.7741
PReLU [35]	23.7645	0.7489
Leaky ReLU [35]	30.0834	0.5979
FReLU [18]	23.1021	0.7623
DPReLU [19]	3.0469	0.9957
SPS-ReLU scale 0.5	2.9571	0.9960
SPS-ReLU scale 1.0	2.9017	0.9961
SPS-ReLU scale 1.5	2.3891	0.9974
SPS-ReLU scale 2.0	2.8457	0.9963

The relatively balanced performance of FReLU indicates that its adjustments for flexibility in handling features of airflow volume data contribute to a marginally better fit, though it still lags behind the optimal activation functions. The DPRELU function stands out significantly, achieving an RMSE of 3.0469 and an  $R^2$  of 0.9957. This remarkable reduction in error and near-perfect fit to the actual values ( $R^2$  approaching 1) underscores DPRELU's superiority in capturing complex and non-linear relationships in airflow volume. The incorporation of deeper parametrization in DPRELU facilitates greater model flexibility and accuracy, making it highly effective for this prediction task.

The SPS-ReLU functions, with varying weight scales, further improve on the model's performance. At a scale of 0.5, the RMSE drops to 2.9571, and the  $R^2$  rises to 0.9960, indicating a highly accurate prediction. As the weight scale increases to 1.0, 1.5, and 2.0, the RMSE continues to decrease, with the lowest error observed at a scale of 1.5 (RMSE = 2.3891,  $R^2$  = 0.9974). This performance underscores the scaling effect's ability to fine-tune the model's sensitivity to complex patterns in the data, resulting in highly precise predictions.

### 3.5. Activation function performance

The performance evaluation of activation functions in Table 8, based on smoothness scores and final training loss, provides critical insights into the trade-offs between function smoothness and model accuracy. The smoothness score reflects how smoothly the activation function transitions across different inputs, influencing the model's ability to generalize, while final training loss measures the model's prediction error during training.

Table 8. Activation Function Performance of Models

Activation Function	Smoothness Score	Final Training Loss
ReLU [35]	[0.43, 8.23, 33.50]	105.9575
PReLU [35]	[0.40, 9.12, 32.74]	98.4465
Leaky ReLU [35]	[0.40, 11.43, 32.50]	90.1188
FReLU [18]	[0.39, 10.24, 33.54]	111.4347
DPReLU [19]	[0.88, 17.84, 38.15]	88.4528
SPS-ReLU scale 0.5	[2.39, 39.02]	120.5627
SPS-ReLU scale 1.0	[1.33, 38.61]	89.7719
SPS-ReLU scale 1.5	[1.55, 38.87]	89.7916
SPS-ReLU scale 2.0	[1.54, 38.63]	85.9919

ReLU, with smoothness scores [0.43, 8.23, 33.50] and a final training loss of 105.9575, demonstrates a relatively low smoothness, especially in the second and third components, which suggests some rigidity in capturing complex patterns. Its higher training loss implies that the model struggles to achieve optimal predictions, indicating that ReLU's zero-gradient behavior for negative inputs hampers the model's learning capacity in this context. PReLU improves upon ReLU with smoother transitions across inputs, reflected in scores [0.40, 9.12, 32.74] and a reduced final training loss of 98.4465. This enhancement suggests that the learnable parameter in PReLU allows the model to adjust to a wider range of input dynamics, resulting in better generalization and lower error.

Leaky ReLU, with scores [0.40, 11.43, 32.50] and a training loss of 90.1188, demonstrates further reduction in error. This reflects the benefits of incorporating a small slope for negative inputs, allowing the model to retain more information during training and improving its prediction capabilities compared to the standard ReLU.

FReLU, however, shows higher final training loss (111.4347) despite slightly better smoothness in [0.39, 10.24, 33.54]. This suggests that while the function transitions more smoothly, it may introduce instability or over-regularization, leading to reduced model accuracy. Dynamic Parametric ReLU (DPReLU) exhibits a notable leap in both smoothness ([0.88, 17.84, 38.15]) and final training loss (88.4528), indicating superior performance. The high smoothness scores imply that DPRELU is adept at managing complex input variations, facilitating a more precise learning process. This leads to the lowest error among the non-SPS functions, demonstrating that DPRELU's dynamic adaptation enhances the model's ability to capture intricate patterns within the airflow volume data.

The Sigmoid Parametric Shifted ReLU (SPS-ReLU) family, particularly with scales of 0.5, 1.0, 1.5, and 2.0, shows a distinct pattern. At a scale of 0.5, the model demonstrates high smoothness ([2.39, 39.02]) but suffers from the highest final training loss (120.5627), indicating over-smoothing, which can lead to loss of essential information during training. However, as the scale increases, smoothness scores moderate, and the final training loss decreases, reaching its lowest value (85.9919) at a scale of 2.0. This balance suggests that moderate smoothing in SPS-ReLU with higher scaling allows the model to capture essential input variations while preventing overfitting or excessive regularization.

The performance analysis of the activation functions within the MLP-ANN model reveals a

nuanced interaction between smoothness scores, final training loss, and predictive accuracy for airflow volume prediction in under-actuated zones. These results underscore the importance of selecting appropriate activation functions that balance generalization and accuracy, especially in a complex predictive environment influenced by occupant behavior and environmental dynamics.

At the core of the discussion lies the understanding that different activation functions introduce unique learning dynamics, which directly affect the model's capability to generalize across varying patterns of airflow volume. ReLU, a baseline activation function, displays moderate performance with smoothness scores of [0.43, 8.23, 33.50] and a final training loss of 105.9575. The inherent limitation of ReLU stems from its inability to activate for negative inputs, leading to a loss of crucial information during training. This shortcoming is particularly visible in its moderate smoothness score, which suggests some rigidity in capturing more complex, non-linear variations in the airflow data. Consequently, the ReLU-based model exhibits an  $R^2$  of 0.7741 and a RMSE of 22.5458, reflecting its limited ability to model the dynamic fluctuations typical in airflow volumes influenced by transient occupant behavior and environmental changes.

When examining PReLU, we observe a slight improvement in generalization, as demonstrated by lower training loss (98.4465) and smoother transitions across input values, reflected in smoothness scores of [0.40, 9.12, 32.74]. The learnable parameter in PReLU allows the function to adjust the slope for negative inputs, thus enhancing its capacity to capture a broader range of input-output relationships. This adaptability mitigates some of ReLU's deficiencies, leading to an  $R^2$  of 0.7489 and RMSE of 23.7645, though PReLU still suffers from suboptimal error reduction, indicating that this activation function, while more flexible, may still not fully capture the complexity of the data.

Leaky ReLU, which introduces a small slope for negative values, significantly improves the retention of information during training. Its lower final training loss (90.1188) relative to ReLU and PReLU, combined with smoothness scores of [0.40, 11.43, 32.50], suggests that it can better handle the non-linearities present in airflow volume dynamics. However, its performance is still limited in comparison to more sophisticated activation functions, as indicated by its relatively high RMSE of 30.0834 and lower  $R^2$  of 0.5979. This suggests that while Leaky ReLU provides better generalization over standard ReLU, it may introduce excess noise that reduces prediction accuracy.

As we move to more advanced functions such as FReLU and DPRELU, we see marked improvements in both smoothness and training loss. FReLU demonstrates smoothness scores of [0.39, 10.24, 33.54] with a final training loss of 111.4347, showing a slight enhancement in flexibility but still struggling with over-regularization, which limits its predictive accuracy. This is reflected in its RMSE of 23.1021 and  $R^2$  of 0.7623. In contrast, DPRELU exhibits a significant leap in both smoothness ([0.88, 17.84, 38.15]) and final training loss (88.4528). The dynamic parametrization inherent in DPRELU allows the model to fine-tune its response to both positive and negative inputs, capturing complex, non-linear relationships with a high degree of accuracy. This is reflected in the remarkably low RMSE of 3.0469 and near-perfect  $R^2$  of 0.9957, demonstrating DPRELU's superiority in modeling intricate airflow volume dynamics within under-actuated zones.

The Sigmoid Parametric Shifted ReLU (SPS-ReLU) family, particularly with scaling factors ranging from 0.5 to 2.0, offers additional insights into the impact of scaling on model performance. At lower scales, such as 0.5, the model demonstrates high smoothness scores ([2.39, 39.02]) but suffers from the highest final training loss (120.5627) and moderate prediction accuracy (RMSE of 2.9571,  $R^2$  of 0.9960), indicating over-smoothing where the model loses critical details necessary for accurate prediction. However, as the scale increases, the model's ability to generalize improves, and the final training loss decreases. At a scale of 1.5, the model achieves the best balance between smoothness and accuracy, with smoothness scores of [1.55, 38.87], final training loss of 89.7916, RMSE of 2.3891, and  $R^2$  of 0.9974. This suggests that moderate scaling enables the model to capture both short-term and long-term patterns in airflow volume with high precision. The slight increase in training loss at the highest scale (2.0), where the final training loss is 85.9919, smoothness scores are [1.54, 38.63], and the RMSE is 2.8457 with an  $R^2$  of 0.9963, suggests that further increases in scaling may lead to diminishing returns or overfitting.

#### 4. Conclusion

This study successfully developed and evaluated a series of activation functions within an MLP-ANN model for predicting airflow volume in under-actuated zones. The analysis demonstrated that advanced activation functions, such as DPRELU and SPS-ReLU with scaling, significantly outperformed traditional functions like ReLU, PReLU, and Leaky ReLU. These advanced functions, particularly

DPreLU and SPS-ReLU with a scale of 1.5, achieved superior predictive accuracy with  $R^2$  values of 0.9957 and 0.9974, and RMSEs of 3.0469 and 2.3891, respectively. The adaptability and flexibility provided by these functions allowed for better handling of the complex, non-linear airflow patterns influenced by occupant behavior and environmental factors in under-actuated zones.

The main achievement of this research lies in demonstrating how the careful selection and tuning of activation functions can lead to substantial improvements in model accuracy and generalization. By fine-tuning the scaling factors and incorporating dynamic parametrization, the model was able to capture intricate patterns in the airflow data that traditional functions failed to model effectively. However, this study also faced some limitations. The focus on a limited set of activation functions, while comprehensive, may not cover all possible variations, particularly hybrid functions that combine characteristics of multiple types. Additionally, the model was trained and tested using a specific dataset, and its generalizability across different environments or airflow systems remains to be fully validated. Another limitation lies in the complexity introduced by hyperparameter tuning for advanced activation functions, which could increase computational time and model optimization challenges in large-scale applications.

For further work, it would be beneficial to explore hybrid activation functions that merge the strengths of different activation paradigms, potentially improving model accuracy further. Additionally, expanding the model's applicability to other environmental conditions and HVAC systems, as well as testing it across varied datasets, could strengthen its generalizability. Another promising direction is the integration of real-time data streams, allowing the model to dynamically adapt to changes in occupant behavior and environmental conditions. Moreover, reducing computational overhead while maintaining high accuracy remains a crucial area for future exploration, particularly in applications requiring real-time predictions and responses.

### Conflicts of Interest

The authors declare that there is no conflict of interest regarding the publication of this research article. No personal circumstances or interests exist that could be perceived as inappropriately influencing the representation or interpretation of the reported research results.

### Author Contribution

Conceptualization, Yaddarabullah and Abiyyu Muhammad Arif; methodology, Dewi Lestari, Budi Arifitama, Dina Nurul Fitria, and Erneza Dewi Krishnasari; software, Abiyyu Muhammad Arif; validation, Yaddarabullah, Aedah Binti Abd Rahman, and Amna Saad; formal analysis, Dewi Lestari; investigation, Yaddarabullah; resources, Yoga Alviando; data curation, Erneza Dewi Krishnasari; writing—original draft preparation, Yaddarabullah; writing—review and editing, Yaddarabullah; visualization, Yaddarabullah; supervision, Aedah Binti Abd Rahman, and Amna Saad; project administration, Yaddarabullah; funding acquisition, Yaddarabullah.

### Acknowledgments

We would like to express our sincere gratitude to all those who contributed to the successful completion of this research. First and foremost, we extend our heartfelt appreciation to our supervisor at Asia e University (AeU) and Universiti Kuala Lumpur (UniKL), Prof. Dr. Aedah Binti Abd Rahman and Ts. Dr. Amna Saad, for their invaluable guidance, encouragement, and insightful feedback throughout the project. We would also like to thank Indonesian Ministry of Education, Culture, Research and Technology for giving research funding and Universitas Trilogi for giving permission to use the library as the object of research.

### References

- [1] M. Fiducioso, S. Curi, B. Schumacher, M. Gwerder, and A. Krause, "Safe Contextual Bayesian Optimization for Sustainable Room Temperature PID Control Tuning", In: *Proc. of the Twenty-Eighth International Joint Conference on Artificial Intelligence*, International Joint Conferences on Artificial Intelligence Organization, pp. 5850–5856, 2019, doi: 10.24963/ijcai.2019/811.
- [2] S.-J. Cao, C. W. Yu, and X. Luo, "Heating, ventilating and air conditioning system and environmental control for wellbeing", *Indoor and Built Environment*, Vol. 29, No. 9, pp. 1191–1194, 2020, doi: 10.1177/1420326X20951967.
- [3] J. Brooks, S. Kumar, S. Goyal, R. Subramany, and P. Barooah, "Energy-efficient control of under-actuated HVAC zones in commercial buildings", *Energy Build*, Vol. 93, pp. 160–168, 2015, doi: 10.1016/j.enbuild.2015.01.050.

- [4] W. Liang, S. Ma, E. Cochran, and K. A. Flanigan, "Distributed MPC-ILC Thermal Control Design for Large-Scale Multi-Zone Building HVAC System", *SIGENERGY Energy Inform. Rev.*, Vol. 3, No. 2, pp. 34–46, 2023, doi: 10.1145/3607114.3607118.
- [5] A. Syahputra, Yaddarabullah, M. F. Azhary, A. B. A. Rahman, and A. Saad, "Occupancy Measurement in Under-Actuated Zones: YOLO-based Deep Learning Approach", *International Journal of Advanced Computer Science and Applications*, Vol. 15, No. 2, 2024, doi: 10.14569/IJACSA.2024.0150277.
- [6] Yaddarabullah, A. A. Rahman, and A. Saad, "Improving ventilation classification in under-actuated zones: a k-nearest neighbor and data preprocessing approach", *Indonesian Journal of Electrical Engineering and Computer Science*, Vol. 34, No. 1, pp. 233–244, 2024, doi: 10.11591/ijeecs.v34.i1.pp233-244.
- [7] M. Taebnia, S. Toomla, L. Leppä, and J. Kurnitski, "Air Distribution and Air Handling Unit Configuration Effects on Energy Performance in an Air-Heated Ice Rink Arena", *Energies (Basel)*, Vol. 12, No. 4, 2019, doi: 10.3390/en12040693.
- [8] H.-J. Kim and Y.-H. Cho, "Optimization of supply air flow and temperature for VAV terminal unit by artificial neural network", *Case Studies in Thermal Engineering*, Vol. 40, p. 102511, 2022, doi: <https://doi.org/10.1016/j.csite.2022.102511>.
- [9] P. Anand, C. Sekhar, D. Cheong, M. Santamouris, and S. Kondepudi, "Occupancy-based zone-level VAV system control implications on thermal comfort, ventilation, indoor air quality and building energy efficiency", *Energy Build*, Vol. 204, p. 109473, 2019, doi: 10.1016/j.enbuild.2019.109473.
- [10] J. H. Lee, H. I. Lee, K. H. Ji, and Y. H. Cho, "Optimal Economizer Control of VAV System using Machine Learning", *E3S Web of Conferences*, Vol. 396, 2023, doi: 10.1051/e3sconf/202339603034.
- [11] D. Wei, J. Ma, H. Jiao, and Y. Ran, "Model predictive control for multi-zone Variable Air Volume systems based on artificial neural networks", *J Process Control*, Vol. 118, pp. 185–201, 2022, doi: <https://doi.org/10.1016/j.jprocont.2022.08.014>.
- [12] A. Cansiz, *4.14 Electromechanical Energy Conversion*, I. B. T.-C. E. S. Dincer, Ed., Oxford: Elsevier, pp. 598–635, 2018, doi: 10.1016/B978-0-12-809597-3.00425-9.
- [13] N. Kulathunga, N. R. Ranasinghe, D. Vrînceanu, Z. Kinsman, L. Huang, and Y. Wang, "Effects of Nonlinearity and Network Architecture on the Performance of Supervised Neural Networks", *Algorithms*, Vol. 14, No. 2, p. 51, 2021, doi: 10.3390/a14020051.
- [14] D. Yang, K. M. Ngoc, I. Shin, and M. Hwang, "DPRReLU: Dynamic Parametric Rectified Linear Unit and Its Proper Weight Initialization Method", *International Journal of Computational Intelligence Systems*, Vol. 16, 2023, [Online]. Available: <https://api.semanticscholar.org/CorpusID:256741906>
- [15] R. Thomas, B. Salmon, D. Holloway, and J. Olivier, "Machine learning classification of metallic objects using pulse induction electromagnetic data", *Meas Sci Technol*, Vol. 35, No. 6, p. 66103, 2024, doi: 10.1088/1361-6501/ad2cdd.
- [16] J. Schmidhuber, "Deep learning in neural networks: An overview", *Neural Networks*, Vol. 61, pp. 85–117, 2015, doi: <https://doi.org/10.1016/j.neunet.2014.09.003>.
- [17] A. Mujhid, S. Surono, N. Irsalinda, and A. Thobirin, "Comparison and Combination of Leaky ReLU and ReLU Activation Function and Three Optimizers on Deep CNN for COVID-19 Detection", in *Frontiers in Artificial Intelligence and Applications*, Vol. 358, 2022. doi: 10.3233/FAIA220369.
- [18] S. Qiu, X. Xu, and B. Cai, "FReLU: Flexible Rectified Linear Units for Improving Convolutional Neural Networks", In: *Proc. of 2018 24th International Conference on Pattern Recognition (ICPR)*, pp. 1223–1228, 2018, doi: 10.1109/ICPR.2018.8546022.
- [19] D. Yang, K. M. Ngoc, I. Shin, and M. Hwang, "DPRReLU: Dynamic Parametric Rectified Linear Unit and Its Proper Weight Initialization Method", *International Journal of Computational Intelligence Systems*, Vol. 16, No. 1, p. 11, 2023, doi: 10.1007/s44196-023-00186-w.
- [20] J. Liang, "A method for the detection of electricity theft behavior based on Xavier weight initialization", In: *Proc. of in Second International Conference on Electronic Information Technology (EIT 2023)*, pp. 767–773, 2023.
- [21] A. Almaleh, R. Almushabb, and R. Ogran, "Malware API Calls Detection Using Hybrid Logistic Regression and RNN Model", *Applied Sciences*, Vol. 13, No. 9, 2023, doi: 10.3390/app13095439.

- [22] S. Basodi, C. Ji, H. Zhang, and Y. Pan, "Gradient Amplification: An Efficient Way to Train Deep Neural Networks", *Big Data Mining and Analytics*, Vol. 3, No. 3, pp. 196–207, 2020, doi: 10.26599/bdma.2020.9020004.
- [23] L. Lu, Y. Shin, Y. Su, and G. E. Karniadakis, "Dying ReLU and Initialization: Theory and Numerical Examples", *Commun Comput Phys*, Vol. 28, No. 5, pp. 1671–1706, 2020, doi: 10.4208/cicp.oa-2020-0165.
- [24] W. Sun, J. Dang, L. Zhang, and Q. Wei, "Comparison of Initial Learning Algorithms for Long Short-Term Memory Method on Real-Time Respiratory Signal Prediction", *Front Oncol*, Vol. 13, 2023, doi: 10.3389/fonc.2023.1101225.
- [25] K. He, X. Zhang, S. Ren, and J. Sun, "Deep Residual Learning for Image Recognition", in *IEEE Conference on Computer Vision and Pattern Recognition (CVPR)*, 2016, pp. 770–778. doi: 10.1109/CVPR.2016.90.
- [26] W. Wang, J. Zhang, M. R. Brambley, and B. Futrell, "Performance Simulation and Analysis of Occupancy-Based Control for Office Buildings With Variable-Air-Volume Systems", *Energies (Basel)*, Vol. 13, No. 15, p. 3756, 2020, doi: 10.3390/en13153756.
- [27] N. Nassif and I. Ridwana, "Improving Building Energy Performance Using Dual VAV Configuration Integrated With Dedicated Outdoor Air System", *Buildings*, Vol. 11, No. 10, p. 466, 2021, doi: 10.3390/buildings11100466.
- [28] Z. Wang, Y. Ding, H. Deng, F. Yang, and N. Zhu, "An occupant-oriented calculation method of building interior cooling load design", *Sustainability (Switzerland)*, Vol. 10, No. 6, May 2018, doi: 10.3390/su10061821.
- [29] J. Lu, J. Huang, and F. Lü, "Time Series Prediction Based on Adaptive Weight Online Sequential Extreme Learning Machine", *Applied Sciences*, Vol. 7, No. 3, p. 217, 2017, doi: 10.3390/app7030217.
- [30] A. S. Al-Khaleefa *et al.*, "Knowledge Preserving OSELM Model for Wi-Fi-Based Indoor Localization", *Sensors*, Vol. 19, No. 10, p. 2397, 2019, doi: 10.3390/s19102397.
- [31] H. Guo *et al.*, "Spatial and Temporal Variations of Air Quality and Six Air Pollutants in China During 2015–2017", *Sci Rep*, Vol. 9, No. 1, 2019, doi: 10.1038/s41598-019-50655-6.
- [32] Z. Peng *et al.*, "Graph Representation Learning via Graphical Mutual Information Maximization", In: *Proc. of The Web Conference 2020*, NY, USA, pp. 259–270, 2020, doi: 10.1145/3366423.3380112.
- [33] M. Mandal, P. K. Singh, M. F. Ijaz, J. Shafi, and R. Sarkar, "A Tri-Stage Wrapper-Filter Feature Selection Framework for Disease Classification", *Sensors*, Vol. 21, No. 16, p. 5571, 2021, doi: 10.3390/s21165571.
- [34] J. He and Z. Zeng, "Efficient Feature Selection via Joint Neural Network and Pruning", in *Frontiers in Artificial Intelligence and Applications*, Vol. 347, IOS Press, 2022. doi: 10.3233/faia220019.
- [35] A. A. Al-Shargabi, A. Almhafdy, D. M. Ibrahim, M. Alghieth, and F. Chiclana, "Tuning Deep Neural Networks for Predicting Energy Consumption in Arid Climate Based on Buildings Characteristics", *Sustainability*, Vol. 13, No. 22, 2021, doi: 10.3390/su132212442.
- [36] G. Krishna, C. Tran, M. Carnahan, Y. Han, and A. H. Tewfik, "Generating EEG features from Acoustic features", in *2020 28th European Signal Processing Conference (EUSIPCO)*, 2021, pp. 1100–1104. doi: 10.23919/Eusipco47968.2020.9287498.
- [37] M. Andorrà *et al.*, "Assessing Biological and Methodological Aspects of Brain Volume Loss in Multiple Sclerosis", *JAMA Neurol*, Vol. 75, No. 10, p. 1246, 2018, doi: 10.1001/jamaneurol.2018.1596.
- [38] B. Das, M. Mondal, B. Lall, S. D. Joshi, and S. D. Roy, "Softmax Gradient Tampering: Decoupling the Backward Pass for Improved Fitting", *CoRR*, Vol. abs/2111.12495, 2021, doi: 10.48550/arXiv.2111.12495.
- [39] S. Ahn, K.-T. Kang, I. Lee, S. Park, Y. Ma, and S. Kang, "Convolutional Neural Network-based Multi-touch Detection Technique on Learning From Class-imbalanced Dataset", *Sid Symposium Digest of Technical Papers*, Vol. 51, No. 1, pp. 1867–1870, 2020, doi: 10.1002/sdtp.14270.